

FEASIBILITY OF USING FRITS AS RAW MATERIALS IN PORCELAIN TILE COMPOSITIONS

A. Moreno, J. García-Ten, V. Sanz, A. Gozalbo

Instituto de Tecnología Cerámica (ITC)
Asociación de Investigación de las Industrias Cerámicas (AICE)
Universitat Jaume I. Castellón. España

J. Cabedo, R. Berge, J. Colom, S. Carmena

Johnson Matthey Ceramics, S.A.

1. INTRODUCTION

Porcelain tile has become a highly valued product in recent years owing to its technical qualities (practically zero apparent porosity, high mechanical strength, frost resistance, low chemical attackability, etc.), and range of aesthetic possibilities (glazed, stained body, etc.)^[1]. The composition of this type of product is basically made up of three raw materials that provide the appropriate plasticity for green processing and the necessary meltability for producing the foregoing end product properties. The basic raw materials involved are white-firing clays, sodium feldspars and feldspathic sands, to which small quantities of pigments are usually added to provide the desired aesthetic finish^[2].

2. OBJECTIVE AND SCOPE

The present work was undertaken to study the feasibility of using non-opaque ceramic frits as fluxing raw materials in porcelain tile compositions. An analysis was performed of how porcelain tile composition properties are altered (sintering range, porosity, glassy and crystalline-phase distribution, etc.), on incorporating one of these frits in different proportions.

[1] BIFFI, G. *Gres porcellanato : tecnologia, produzione, mercato*. Faenza: Faenza Editrice, 1994.

[2] SÁNCHEZ, E.; GARCÍA, J.; SANZ, V.; OCHANDIO, E. *Criterios de selección de materias primas para la fabricación de pavimentos y revestimientos cerámicos*. *Cerám. Información*, 157, 13-21, 1990.

3. EXPERIMENTAL

3.1.- MATERIALS

A standard industrial porcelain tile composition was used (STD). The composition, whose chemical analysis is given in Table 1, is formulated with a white-firing kaolinitic-illitic clay, sodium feldspar and feldspathic sand. An industrial frit was used, which yields transparent glazes. The major oxides in the frit composition were SiO₂, B₂O₃, Na₂O, CaO y Al₂O₃.

SiO ₂	Al ₂ O ₃	Fe ₂ O ₃	CaO	MgO	Na ₂ O	K ₂ O	TiO ₂	ppc
69.0	19.4	0.49	0.53	0.29	4.54	1.28	0.58	3.65

Table 1. Chemical composition of the STD composition (wt%)

3.2.- EXPERIMENTAL PROCEDURE

3.2.1.- Composition preparation

Table 2 details the compositions prepared. In general lines, the differences lie in the progressive incorporation of the frit in the starting composition up to a proportion of 12%.

Owing to the rise in price that would be involved in adding frit to the composition, the relative proportions of the starting raw materials were modified in composition M-103, partially replacing the more expensive ones (feldspar and clay) by the cheaper sand. The rise in raw materials cost entailed by a 4% frit addition was thus compensated.

Composition M-103 was then used to prepare two further compositions (M-104 and M-105) by incorporating larger quantities of frit (8% and 12%) and correspondingly reducing the feldspathic sand content.

	STD	M-103	M-104	M-105
Clay	45	40	40	40
Sodium feldspar	45	21	21	21
Feldspathic sand	10	35	31	27
Frit	0	4	8	12

Table 2. Prepared compositions (wt%).

The procedures used to prepare the compositions are set out below.

The frit was first wet milled in a planetary ball mill until a residue of 1-2% was

obtained on a 63- μm -mesh screen. 5% kaolin was added to facilitate milling. The suspension obtained was oven dried at 110°C. The resulting material was then comminuted in a cross beater.

The compositions were prepared by mixing the different raw materials in suitable proportions (Table 2). These blends were wet milled in a planetary ball mill until a residue of 1.5-2% was obtained on a 63- μm -mesh screen. The resulting suspensions were dried and comminuted by an analogous procedure to the above.

3.2.2.- Pressing and firing

Composition behaviour during the pressing stage was studied by forming test specimens at a 5.8% moisture content (on a dry basis), using various pressing pressures. The test specimens were then dried, determining bulk density by the mercury immersion method.

To determine how the frit addition affected the behaviour of the compositions during firing, the evolution of the following characteristics with temperature were determined:

- Linear shrinkage (LS)
- Water absorption (WA)
- Bulk density (D_{ap})
- Pyroplasticity index (PI)

The determination of shrinkage, water absorption and density of the compositions was conducted on 6-mm-thick, cylindrical test specimens with a 40-mm diameter, while the pyroplasticity index was measured using prism-shaped test specimens sized 80x20x6 mm. The above properties were determined on specimens pressed at a 5.8% moisture content and constant dry bulk density of 1.950 g/cm³. In this way, the influence of compactness on the development of this process stage was eliminated.

The firings were run at different peak temperatures in an electric laboratory kiln using the following firing schedule:

- heating rate from 500°C to peak temperature: 25°C/min
- residence time at peak temperature: 6 minutes
- cooling: forced convection (50 °C/min)
- heating rate up to 500°C: 95°C/min

The total firing cycle duration was 60 minutes.

It should be noted that in determining the pyroplasticity index, the test specimens only rested on their ends, so that they could deform during firing.

The following equations were used to calculate the characteristics set out above:

$$LS = \frac{l_s - l_c}{l_s} \cdot 100 \qquad WA = \frac{m_a - m_c}{m_c} \cdot 100$$

$$D_{ap} = \frac{m \cdot D_{Hg}}{e_p} \qquad PI = \frac{4 \cdot e^2 \cdot S}{3 \cdot L^4}$$

where:

- l_s: dry specimen diameter (mm).
- l_c: fired specimen diameter (mm).
- m_a: fired specimen mass after immersion in a thermostatted bath with boiling water for 2 hours (g).
- m_c: fired specimen mass (g).
- m: dry or fired specimen mass (g).
- D_{Hg}: mercury density (13.53 g/cm³).
- e_p: specimen upthrust in mercury (g).
- e: specimen thickness (cm).
- S: sag (cm).
- L: spacing between supports (cm).

3.2.3.- Porous structure of the materials

To study the influence of the frit on the porous structure of the resulting materials, the specimens fired at the temperature yielding maximum densification were chosen. They were polished with an abrasive using progressively finer grain, first with silicon carbide, then with diamond, and finally using an abrasive with a mean grain size of 1 μm. The appearance of the polished surfaces was observed on a stereoscopic microscope fitted with a camera, photographing a representative area of each specimen. The specimens were observed with direct, completely superficial lighting (clear field) to point up any irregularities such as cracks, pores, crystals or grain edges, which take on a black colour in the picture.

These same specimens were used to determine pore size distribution by image analysis. This was done by classifying the pores in 50 classes, of equal size on a logarithmic scale, quantifying the number of pores in each class. The area of each was calculated from the number of existing pores and the mean diameter assigned to each class, making the assumption that spherical pores were involved. To achieve greater data accuracy, 30 screens were measured of each tested specimen.

Cross sections of the specimens fired at different temperatures were also examined by scanning electron microscopy (SEM) to determine how microstructure evolved with temperature.

3.2.4.- Nature and composition of the phases present

The crystalline phases were identified and quantified on a Philips, X'Pert, X-ray diffraction instrument. This was done by previously determining the calibration straight lines of the crystalline phases present in the specimens, using fluorite as an internal standard. The quantity of identified crystalline phases was then estimated, by measuring integrated peak intensity with a deconvolution software.

Finally glassy-phase proportion and composition were calculated from the difference between the composition of the calcined sample and that of the detected crystalline phases.

4. RESULTS AND DISCUSSION

4.1.- BEHAVIOUR IN THE PRESSING AND FIRING STAGES

The evolution of test specimen dry bulk density with applied pressure is presented in Figure 1. The figure shows that specimen bulk density dropped slightly as larger quantities of frit were added, which meant raising pressure a little to attain working compactness. This behaviour is to be associated with frit particle-size distribution (PSD). As frit PSD exhibited an intermediate diameter (around 10 μm) and a narrow distribution, intermediate particle content increased to the detriment of the large and small-size particles, which lowered composition packability ^[3].

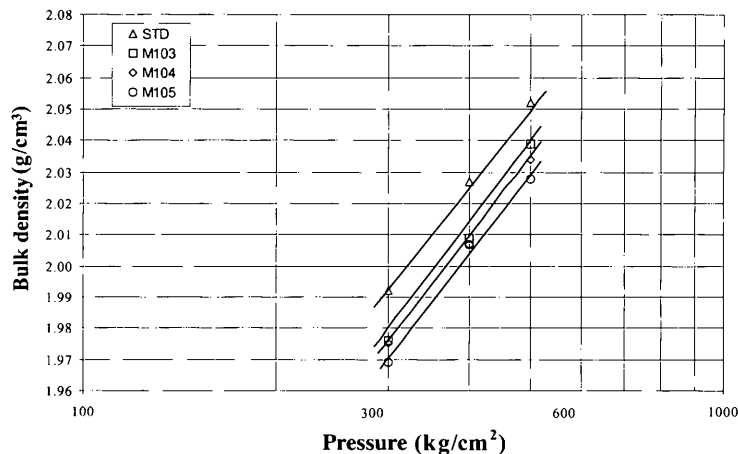


Figure 1. Compaction diagrams

Figure 2 plots the variation of specimen bulk density and water absorption with peak firing temperature. The figure shows that the STD and M-103 compositions exhibited very similar meltability, as the curves corresponding to the evolution of water absorption with temperature are practically identical. This indicates that the meltability provided by the 4 % frit addition compensated the drop in sodium feldspar content (24%) together with the increase in feldspathic sand content (25%).

The successive substitutions of feldspathic sand by frit in the M-103 composition, which yielded compositions M-104 and M-105, progressively shifted the

[3] SANCHEZ, E.; GARCÍA-TEN, J.; BARBA, A.; BELTRÁN, V. Estimation of packing density of raw material mixtures used in tile manufacture. Br. Ceram. Trans., 97(4), 149-154, 1998.

WA-T curves towards lower temperatures, revealing the fluxing effect of the frit added to this type of composition. This fact could be used to manufacture porcelain tile at low temperatures (similar to those used for red-firing compositions) or shorten current firing cycles.

The curves plotting the variation of specimen bulk density with firing temperature show that the effect of the frit coincided with the above-mentioned effect. Thus, while the Dap-T curve of composition M-103 did not shift to lower temperatures, this effect is observed for compositions M-104 and M-105. As a further effect, specimen bulk density fell, which became more pronounced as frit content rose. This can be appreciated more clearly in Table 3, where specimen properties at maximum densification temperature (T_{max}) are given.

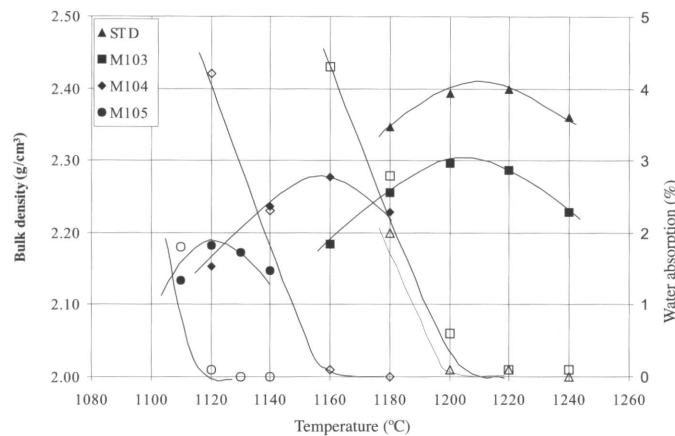


Figure 2. Evolution of bulk density and water absorption with firing temperature.

	STD	M-103	M-104	M-105
T_{max} (°C)	1212	1206	1160	1125
D_{ap} (g/cm ³)	2.401	2.297	2.274	2.182
LS (%)	6.9	5.8	5.6	4.4
WA (%)	0.0	0.0	0.0	0.0
ϵ_c (%)	5.8	9.9	10.8	14.4
$IP \cdot 10^5$ (cm ⁻¹)	4.4	4.6	6.3	7.5

Table 3. Specimen properties at maximum densification temperature.

The water absorption (WA) and fired bulk density (D_{ap}) data were used to calculate apparent porosity (ϵ_a), true porosity (ϵ_T) and sealed porosity (ϵ_c) of the materials from the following equations:

$$\epsilon_a = AA \cdot D_{ap} \qquad \epsilon_T = 1 - \frac{D_{ap}}{D_R} \qquad \epsilon_c = \epsilon_T - \epsilon_a$$

where D_R is specimen true density. It should be noted that given the zero water absorption in every case, apparent porosity will be zero, so that sealed porosity will coincide with true porosity.

These results, also included in Table 3, indicate that the frit addition yields an increased volume of sealed porosity in the specimens fired at maximum densification temperature. This fact is in turn responsible for decreased specimen shrinkage.

Table 3 also presents the pyroplasticity index values of the specimens at maximum densification temperature (T_{\max}). The magnitude of this deformation depends on the force acting on the specimens (in this case the force of gravity) and their apparent viscosity. Apparent viscosity is a function of the liquid-phase/crystalline-phase ratio in the materials as well as liquid-phase viscosity.

In this type of composition, the first viscous liquid phases start arising from 900-1000°C on. Liquid-phase viscosity decreases with rising firing temperature, which favours the progressive dissolution of the remaining minerals in the body. This all makes the variation of the pyroplasticity index with temperature follow an exponential trend ^[4].

The PI data (Table 3) show that the frit addition increased the tendency to deform pyroplastically. This rise, which was not significant for 6% frit additions, increased noticeably when the frit addition exceeded 8%. The differences found are to be attributed either to the quantity of liquid phase present in the specimens, or to the variation of liquid-phase viscosity on incorporating the frit. These aspects are dealt with below.

4.2.- EVOLUTION OF POROUS STRUCTURE

Figures 3 to 6 present the images corresponding to the porous structure of the materials at maximum densification temperature. The frit addition can be observed to yield a microstructure with a larger pore volume, which is consistent with the lower bulk density exhibited by the specimens. Moreover, the frit addition altered specimen porous structure, giving rise to a system of considerably larger-sized, isolated pores. This tendency became more pronounced as the frit addition increased. Figure 7 plots specimen pore size distribution. The figure reveals that raising the frit content of the composition produced the following changes in the porous structure:

- The most frequent pore diameter shifted to larger sizes.
- The percentage of small pores (under 10 μm) decreased.
- The percentage of large pores (between 20 and 100 μm) increased.

In order to determine what caused this microstructural change, the evolution of composition STD and M-105 specimen microstructures with peak firing temperature was monitored by scanning electron microscopy (SEM). The M-105 composition was chosen because of its larger frit content, which allowed more clearly observing the effect of the frit presence on specimen porous structure.

Figures 8 to 11 illustrate the evolution of STD composition specimen microstructure with firing temperature (1150, 1175, 1200 and 1225°C).

The specimen fired at 1150°C exhibits a great number of pores, which form an interconnected capillary network. The large variety of pore sizes, their irregular shape, and the presence of particles with sharp edges, are characteristic of the initial stages of the liquid-phase sintering process that develops during porcelain tile firing. As temperature rises (1175°C), liquid phase becomes progressively less viscous and is able to eliminate

[4] ESCARDINO, A.; AMORÓS, J.L.; NEGRE, F.; FELIU C. *Defectos de planaridad en las piezas de pavimento gresificado motivadas por deformación piropástica. Influencia de las variables del proceso.* Cerám. Cristal, 102, 38-43, 1988.

larger pores. The number of small-size pores thus decreases, while the larger-size pores become more isolated and start acquiring a rounded shape. At the working temperatures for these compositions (1200°C), the structure exhibits a highly densified appearance, containing isolated, highly rounded pores. Finally, when the temperature is raised further (1225°C), the pressure of the gases trapped in the pores exceeds liquid-phase surface tension, enlarging and spherizing the pores, producing bloating.

Figures 12 to 17 present the evolution of M-105 composition specimen porous texture on modifying firing temperature (700, 850, 1000, 1075, 1100 and 1125°C). At low temperatures (700°C) all the particles, including the frit particles are individualised and exhibit sharp edges, indicating that the sintering process has not yet started. The pores in the specimen are extremely small, highly connected, inter-particle pores. The presence is also detected of certain spherical pores inside the frit particles, stemming from the fritting process.

At 850°C, the frit has started melting, cementing the surrounding particles. Thus, in the areas where frit particles are found, clusters of welded particles can be observed, where the first spherical pores have developed. These pores arise, either as a result of the growth of pores present inside the frit particles, or owing to trapped air bubbles inside the regions with welded particles.

At 1000°C, the particles are totally welded. Many small-size pores have been eliminated, while the large ones have coalesced, forming large, irregular pores. At this temperature, there are two types of pores:

- a) Small, irregular, interconnected pores in areas where porcelain tile composition particles predominate.
- b) Large pores with rounded edges in the proximity of frit particles.

If temperature is raised further (1075°C and 1100°C), the small, interconnected pores are progressively eliminated. Finally, at maximum densification temperature (1125°C) the specimen microstructure exhibits greater porosity than the STD composition specimen and only contains large, isolated, spherical pores.

Summing up, the incorporation of the frit into the porcelain tile compositions modified the sintering process in certain micro-regions of the body. Thus, while the compositions without the frit particles sintered analogously to the STD composition, the areas adjacent to the frit particles sintered at a notably higher rate as a result of the point generation of not very viscous liquid phase at low temperatures (800°C). This liquid phase from the melting frit trapped bubbles of air during the cementing process with the surrounding particles. This fact, together with the existence of porosity inside the frit particles themselves, gave rise to the formation of large-size, isolated pores at porcelain tile firing temperature.

4.3. TYPE AND PROPORTION OF PHASES PRESENT

The nature and proportion of the crystalline phases present in the green specimens are listed in Table 4. The following phases were present: illite and kaolinite - associated with clay; albite - provided by feldspar; orthoclase - present in feldspathic sand; quartz - from feldspathic sand and to a lesser extent from clay and feldspar.

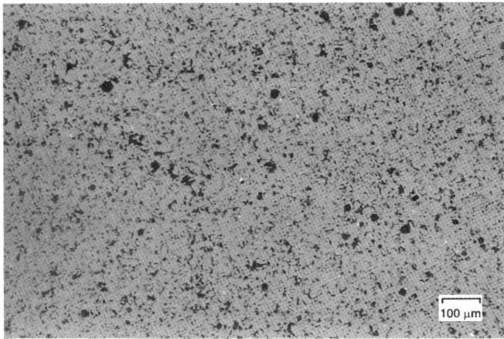


Figure 3. STD composition. 1212 °C

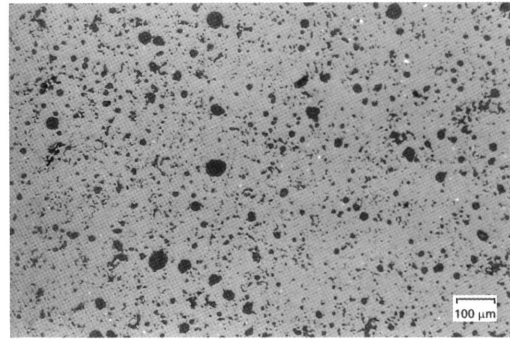


Figure 4. M-103 composition. 1206 °C.

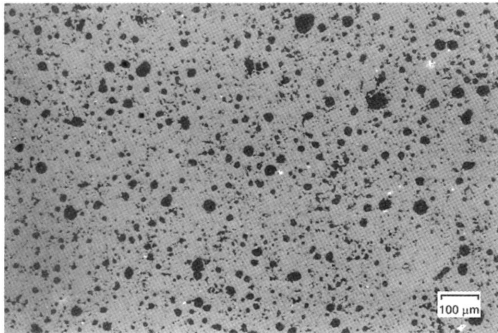


Figure 5. M-104 composition. 1160 °C

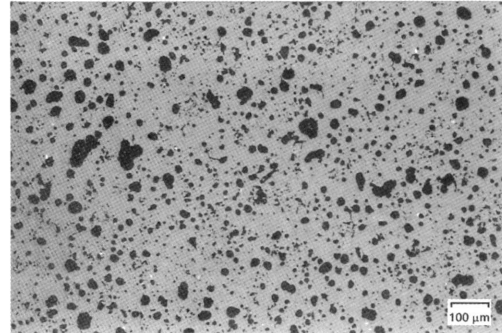


Figure 6. M-105 composition. 1120 °C

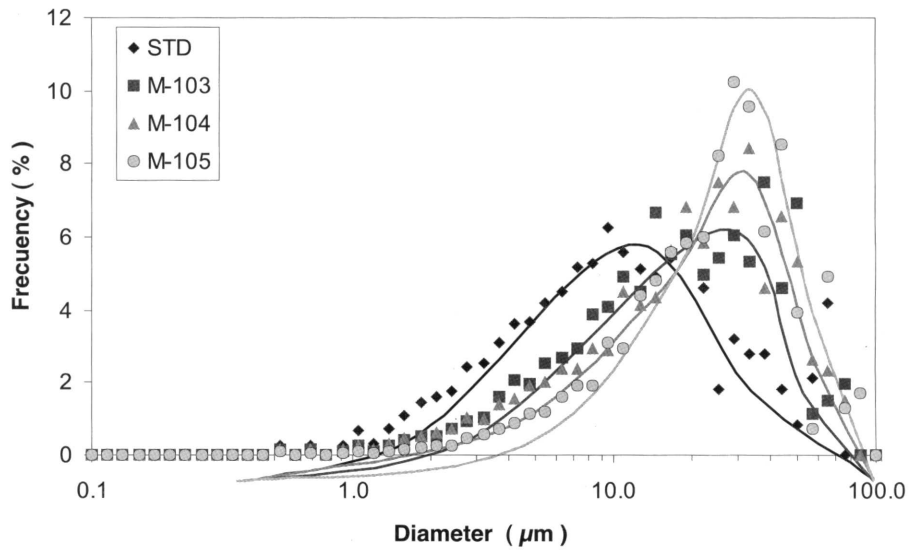


Figure 7. Pore-size distribution.

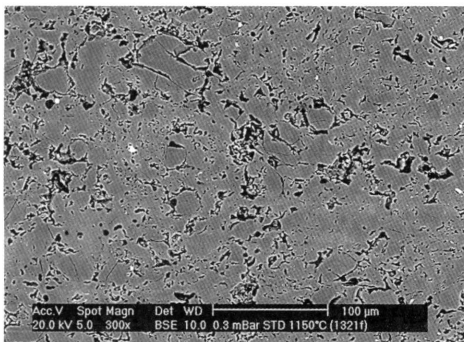


Figure 8. STD composition. 1150 °C

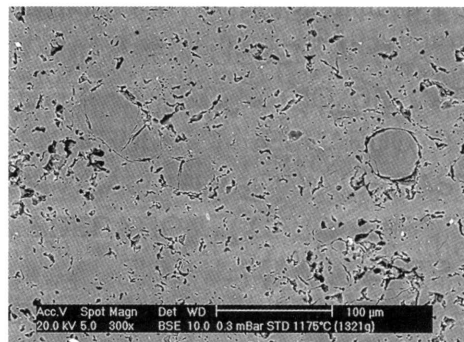


Figure 9. STD composition. 1175 °C

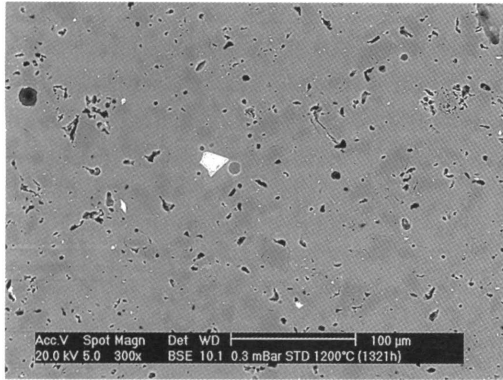


Figure 10. STD composition. 1200°C

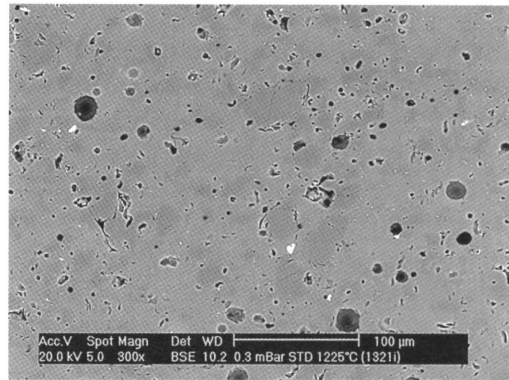


Figure 11. STD composition. 1225°C

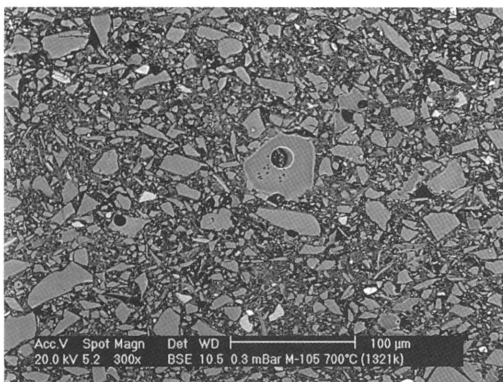


Figure 12. M-105 composition. 700°C

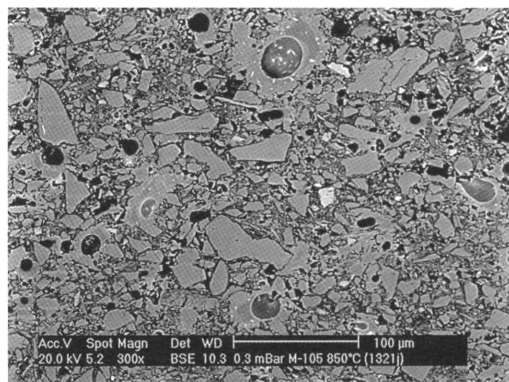


Figure 13. M-105 composition. 850°C

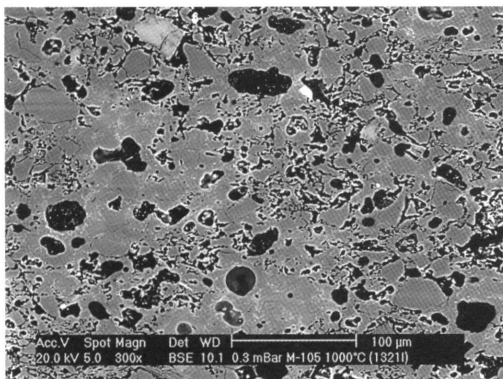


Figure 14. M-105 composition. 1000°C

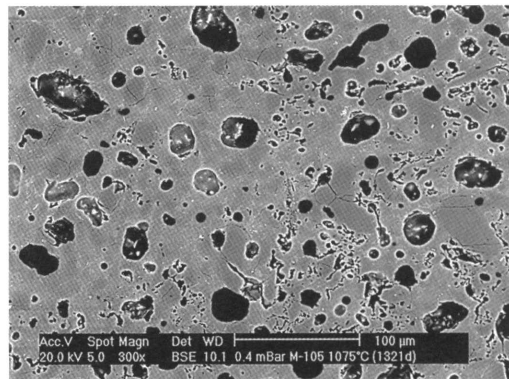


Figure 15. M-105 composition. 1075°C

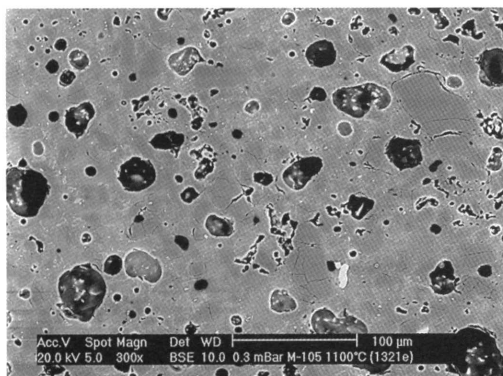


Figure 16. M-105 composition. 1100°C

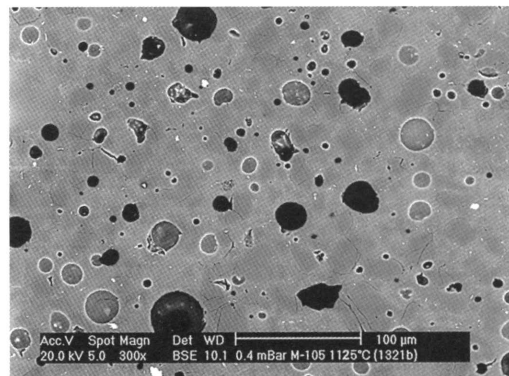


Figure 17. M-105 composition. 1125°C

The substitution of feldspathic sand by frit (glassy phase) was observed to lead to a drop in the total quantity of crystalline phases, mainly due to the smaller proportion of quartz in the specimens.

	STD	M-103	M-104	M-105
Quartz	27.4	45.3	41.7	38.2
Kaolinite	21.9	19.7	19.6	19.6
Illite	7.3	6.6	6.5	6.3
Albite	39.2	19.2	19.2	19.2
Orthoclase	2.4	3.7	3.5	3.2
Total crystalline phases	98.2	94.5	90.5	86.5

Table 4. Crystalline phases present in the green specimens (% on the whole composition).

Table 5 lists the content of the different crystalline phases in the specimens at maximum densification temperature. While only residual quartz and mullite were detected in the specimens corresponding to compositions STD and M-103, in the other compositions the presence of residual albite was also found. This was because the low firing temperatures of these compositions were not sufficiently high for albite to melt completely.

	STD	M-103	M-104	M-105
Quartz	17.9	24.9	24.0	21.6
Albite	0.0	0.0	1.5	3.2
Mullite	6.6	4.5	3.1	1.5

Table 5. Crystalline phases at maximum densification temperature (% on the whole composition).

The evolution of the mullite content is plotted in Figure 18. The figure shows that for the STD composition, raising firing temperature increased the mullite content which peaks at around 1190°C. Above this temperature a slight drop is detected, as this crystalline phase redissolves in the abundant liquid phase contained in the specimen ^[5 y 6].

Although the frit addition did not alter this tendency, it made the curves shift to lower temperatures, indicating that the arising mullite redissolved at lower temperatures. Moreover, peak mullite content dropped as frit quantity rose. Both effects are the result of the presence of a greater proportion of low-viscosity glassy phase at relatively low temperatures in the frit-bearing specimens. This encouraged the dissolution of silica and alumina from clay mineral decomposition, which reduced the amount of mullite that could form. On the other hand, the early presence of liquid phase favoured redissolution of the mullite that formed at low temperatures.

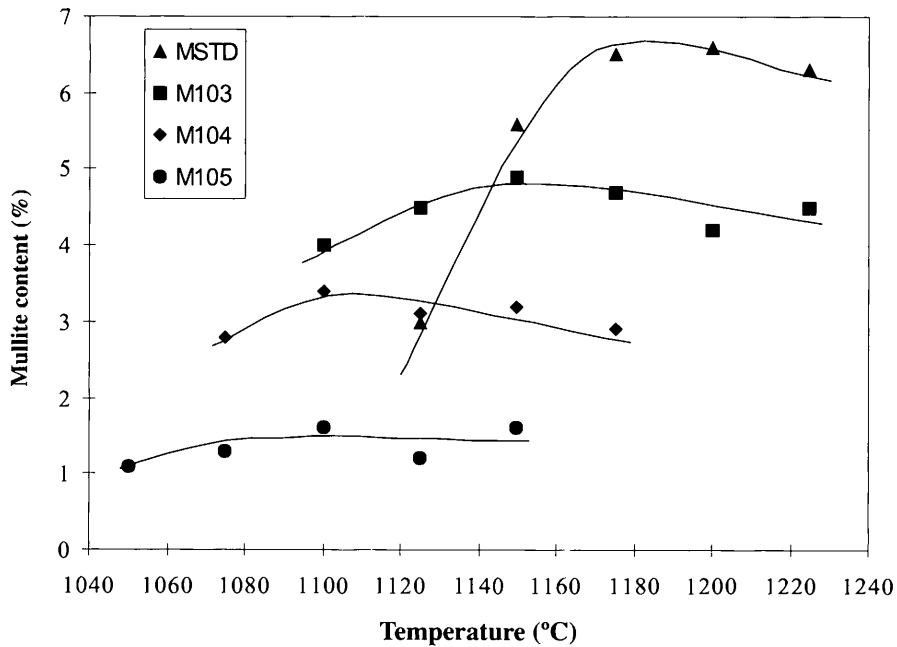


Figure 18. Evolution of mullite content with firing temperature.

Figure 19 plots the evolution of liquid-phase (LP) content of the different compositions with firing temperature. For all the studied compositions, the liquid-phase content rose with increasing temperature owing to the progressive dissolution of the other constituents in the melt. If only the frit-containing compositions are compared (M-103, M-104 and M-105), the progressive frit addition was found to raise glassy-phase content at a given temperature, owing to the larger glass content (frit) in the starting composition. On the other hand, the greater liquid-phase content of the STD compared to the M-103 composition is to be associated with the pronounced drop in M-103 feldspar content.

Table 6 sets out the percentage and composition of the liquid phase in the specimens fired at maximum densification temperature. A comparison of the frit-containing compositions shows that the frit addition slightly raised liquid-phase content, which was enriched in oxides B_2O_3 , Na_2O , CaO , MgO and Al_2O_3 contained in the frit and made poorer in SiO_2 . This compositional change produced a drop in liquid-phase viscosity^[7], which, together with a greater liquid-phase quantity, caused faster body vitrification with progressive frit addition, thus making it possible to reduce porcelain tile firing temperatures.

[5] WARSHAW, S.I.; SEIDER, R. *Comparison of strength of triaxial porcelains containing alumina and silica*. Journal of the American Ceramic Society, 50(4), 337-343, 1967.

[6] KRISTOFFERSSON, A.; EKBERG, I.L.; LEANDERSSON, H.; CARLSSON, R. *High strength triaxial porcelain by an improved glassy phase*. International Ceramics Journal, June, 42-45, 1994.

[7] FERNÁNDEZ NAVARRO, J.M. *El vidrio: constitución, fabricación, propiedades*. 2ª ed. Madrid: CSIC, 1991.

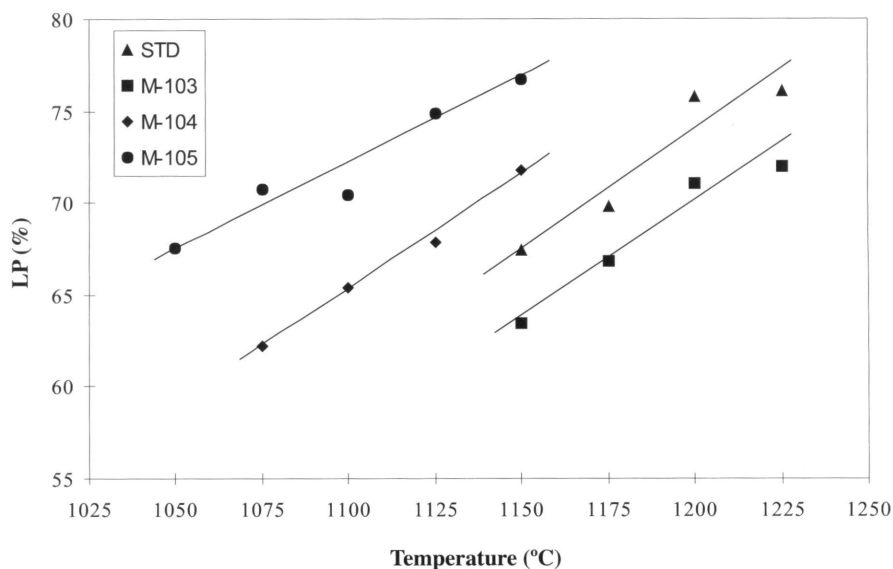


Figure 19. Evolution of the liquid-phase proportion with firing temperature.

With regard to the STD and M-103 compositions, the lower liquid-phase content of the M-103 composition appeared to be compensated by its lower viscosity, thus not significantly altering firing temperature.

	STD	M-103	M-104	M-105
LP (%) ^(*)	75.5	70.6	71.4	73.8
SiO ₂	68.6	71.6	67.8	64.7
Al ₂ O ₃	20.5	17.4	18.7	19.6
B ₂ O ₃	-	1.3	2.5	3.6
Na ₂ O	6.3	4.4	5.2	5.8
K ₂ O	1.8	2.1	2.0	1.9
CaO	0.7	1.0	1.4	1.7
MgO	0.4	0.7	0.9	1.2

(*) Porcentaje respecto al total de la composición.

Table 6. Liquid-phase proportion and composition at maximum densification temperature.

4.4.- INDUSTRIAL APPLICATION

In view of the laboratory-scale findings, which confirmed the effectiveness of the studied frit as a fluxing raw material in porcelain tile compositions, it was decided to run a series of industrial trials to verify the results on an industrial scale.

The first industrial trial was performed to reduce the firing temperature of a composition used for manufacturing glazed porcelain tile. To facilitate the incorporation of the frit into the composition, the frit was milled beforehand and added as a suspension to the spray-dryer feed tanks. A 7% frit addition was used. The industrial process variables were held unchanged during the trial, with the logical exception of roller kiln peak firing temperature.

On monitoring this trial, no type of production problem was detected in any of the different stages making up the process. Nor were any faults found in the fired products associated with the presence of the frit (curvature, deformation, etc.). Table 7 lists kiln peak firing temperatures and water absorption of the resulting products.

	Industrial kiln temperature (°C)	Water absorption of the product (%)
STD	1200 °C	0.5
STD+7% frit	1150 °C	0.3

Table 7. Results obtained in the first industrial trial.

The table shows that a 7% frit addition to the standard industrial composition enabled obtaining a product with the same water absorption (0.5%) at a noticeably lower peak firing temperature, which dropped from 1200°C to 1150°C.

Certain preliminary tests were conducted before running the second industrial trial, designed to make glazed porcelain tile with a standard white-firing porcelain tile composition without changing the process variables (mainly peak firing temperature and the cycle). In this case a 4.0% frit addition was used.

Table 8 sets out the results. The fluxing effect of the studied frit can again be observed, which allows using a single composition to make a variety of products with different degrees of vitrification relatively easily, ranging from stoneware floor tile with a water absorption of less than 3.0% to glazed porcelain tile with a water absorption of less 0.5%.

	T (°C)	Cycle (min)	LS (%)	WA (%)
STD	1160	55	6.1	2.8
STD+4% frit	1160	55	6.6	0.1

Table 8. Results obtained in the preliminary test run prior to the second industrial trial.

5. CONCLUSIONS

The study allowed drawing the following conclusions:

- Incorporating small percentages of the studied frit produced a rise in porcelain tile composition meltability. This can be used to significantly lower the peak firing temperature of these products, or shorten current firing cycles.
- Although this frit addition did not alter the nature of the crystalline phases present in the fired product, it lowered the quartz and mullite content, and at high frit additions raised the albite content. Moreover, the amount of liquid phase in the end product increased slightly and changed in composition.

- Adding this frit was found to yield a product with a more porous microstructure, containing larger-size, isolated pores. Although this was not confirmed in this study, the microstructural change could detrimentally affect polished porcelain tile stain resistance, so that the industrial use of this frit would appear most appropriate for glazed products.

- It was confirmed by an industrial trial that using this frit as a fluxing raw material is technically feasible, as it noticeably reduces porcelain tile firing temperature. This facilitates making this type of product with the industrial facilities available at most manufacturers of ceramic redware. The use of this frit would also allow making glazed porcelain tile from the compositions used for manufacturing white-firing stoneware floor tile without modifying the usual process variables in this type of facility.